PCCP

Accepted Manuscript

This article can be cited before page numbers have been issued, to do this please use: V. grivickas, P. Scajev, V. Bikbajevas, A. V. Mazanik and O. Korolik, *Phys. Chem. Chem. Phys.*, 2018, DOI: 10.1039/C8CP06209A.

ROYAL SOCIETY OF CHEMISTRY

rsc.li/pccp

View Article Online
DOI: 10.1039/C8CP06209A

Carrier dynamics in highly-excited $TlInS_2$: Evidence of 2D electron-hole charge separation at parallel layers

Vytautas Grivickas, *[a] Patrik Ščajev,[a] Vitalijus Bikbajevas,[a] Olga V. Korolik,[b] and Alexander V. Mazanik[b]

[a] Institute of Photonics and Nanotechnology, Vilnius University, Saulėtekio av. 3, 10257 Vilnius, Lithuania
[b] Energy Physics Department, Belarusian State University, Nezavisimosti av. 4, 220030 Minsk, Republic of Belarus

*E-mail: vytautas.grivickas@ff.vu.lt , phone +370 614 45311

Abstract
We report a comprehensive study of the time-resolved photoluminescence (PL), carrier recombination, and carrier diffusion under diverse laser pulse excitations in $TlInS_2$. The 2D-layered crystals were grown by Bridgman method without or by a small *Erbium* presence in the melt. The investigation expose large differences in two crystal types, although, a linear nonradiative lifetime and carrier diffusivity attain close values at high excitation with no contribution of the Auger recombination and absence of the band gap narrowing effect. Moreover, at high pulse power, we detect imprinted transient grating fringes which are attributed to new crystal phase formed by 2D electron-hole charge separation on local layers. The versatile model of the spontaneously polarized 2D-crystal has been developed to explain observed features and ergodicity of charge dynamic processes. The model embraces the planar stacking faults (PSFs) as a distortion which edge is acting as sink of strong recombination. The reduced occurrence of the PSFs in the *Erbium* doped $TlInS_2$ is the main attribute which determines enhancement of PL by a factor of 50, and improves carrier diffusion along 2D-layers. The simulation permits to evaluate the PSFs sizes of about 0.7 μm. Presented results allow improving 2D-crystal growth technology for novel sensor devices with separated excess charges.

Keywords: 2D-layered structure, photoluminescence, recombination, transient grating, transport of intrinsic excitons, planar stacking faults, charge localization.

1. Introduction

Thallium based ternary dichalcogenides, akin to $TlInS_2$, belong to the class of specific 2D multilayered crystals which obey quite unique properties and attract extensive research interest.[1] The distinct anisotropy in $TlInS_2$ resistivity,[1,2] optical birefringence,[3,4] magneto-dielectric properties,[5] thermal compressibility [1,6] and band edge absorption [7] in conjunction with crystal phases transitions were reported. Several studies showed that anisotropy effects are the peculiarity of 2D-layered structure. Figure 1 presents fragments of atomic stacking in the paraelectric P-phase of the $TlInS_2$ crystal at 300 K. The structure is described by centre-symmetric monoclinic metrics of the C_{2h}^6 group with two layers consisting of 16 atoms per primitive cell.[1] The layers are composed of the rigid In_4S_{10} corner-connected polyhedral stack oriented in the basal {001} direction, with an ionic bond lengths of about 0.15 nm. Each layer is alternately twisted by a right angle around c-axis. In this way, the adjacent layers become shifted relative to each other in a quarter of the cell unit along [1,1,0] or [1,−1,0] direction. The Tl^+ cations take force of interlayer bonding. They are arranged in the trigonal cavities on lines in the above-mentioned directions. Due to the weakness of Tl-S bonds (bond lengths is about 0.35 nm), the crystals can be easily cleaved by a razor blade along the layer. On cooling the $TlInS_2$ crystal loses inversion center undergoing two sequential transitions via incommensurate I-phase into ferroelectric F-phases. Tl^+ ion deviation and

View Article Online
DOI: 10.1039/C8CP06209A

grouping occurs in the interlayer [8,9] and the I-phase is accompanied by strong resonance of complex dielectric function.[10] The lattice unit quadrupling within I-phase occurs around 200 K.[5] Weakness of interlayer bonds results from the sp-hybridization of the Tl electrons wave function where a strong coupling among the spins of Tl and In metal ions on neighboring layers is observed. These couplings were first discovered by the nuclear magnetic resonance.[11-13] The interlayer wave function overlap is the important mechanism in the formation of the valence band maximum (VBM) and the conduction band minimum (CBM) and determines the electronic structure of the compound.

Recently, unexpected polarization phenomena were discovered in ternary 2D-dichalcogenides after maintenance crystals in the I-phase or thermocycling them under external transverse electric fields.[1,6] In addition, asymmetric photocurrent and changes in pyroelectricity were detected in combination with these treatments.[14] Since similar behavior was observed in the isostructural $TlGaSe_2$,[15] these effects were generally described as a kind of 2D-crystal memories caused by giant Stark effect. Due to the observed phenomena, the ternary Tl-dichalcogenides provoke a new great interest in their application for next-generation bulk information storage, energy conversion and optoelectronic sensors. It was suggested that so called planar defect-density-wave perpendicular to the crystal layers or/and an imprinted electric field can form electrets that change physical crystal parameters.[15,16] However, no reasonable explanation in the frame of layered crystal model has been suggested so far.

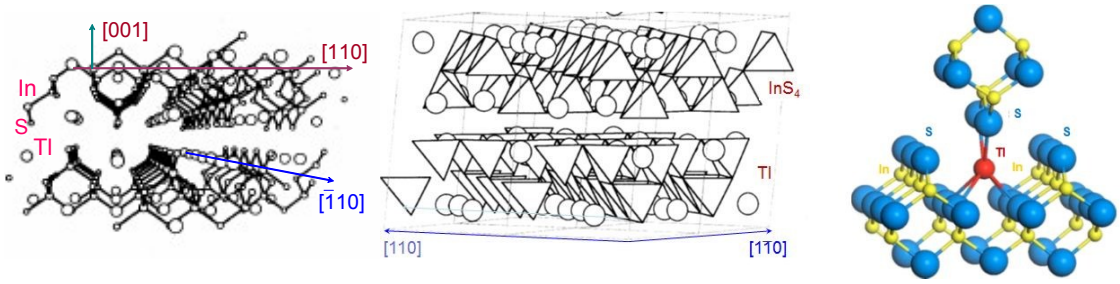

Fig. 1. Stereographic presentations of the $TlInS_2$ layered crystal structure in the paraelectric P-phase at RT. Tl-S atoms skew interlayer bonds are shown by red in (c) and are omitted for clarity in (a, b) fragments.

The planar stacking faults (PSFs) are assumed to be commonly defects in Tl-chalcogenides due to gliding of one part of the crystal by 0.5 lattice units relative to another along the layer plane. Further gliding by 0.5 unit in the same direction will return crystal into previous configuration. The PSFs can make invariant of *a* to *b* axis, e.g. this shifting can lead to tilting monolithic structure from [110] to [1-10]. Even though the PSFs cannot be associated with broken bonds, the PSFs edges may give rise to different stresses and band gap states.

The PSFs were identified by x-ray scattering in the $TlGaSe_2$ compound. Authors suggested that fault occurs in the crystal about once every four layers on average.[20] It is believed that the PSFs presence provides distinct dark resistivity anisotropy.[1,2,21] The deep carrier traps were identified by ordinary photo-induced current transient spectroscopy (PICTS) [16] and by thermally-stimulated current.[22] The trap defect concentration was moderate, in the range of 10^{15}-10^{16} cm^{-3}. Some centers with large cross-section were assigned to presence of the PSFs.[16,21]

It is known that pristine $TlInS_2$ crystal is an inefficient PL emitter, particularly for normal to layers excitation, at k||c.[23,24] This is attributed to presence of the indirect optical band gap. The energies for lowest direct exciton and indirect band gap at RT are E_x^d = 2.44 eV and E_g^i = 2.26 eV, respectively.[24,25] Besides, the direct exciton absorption is relatively low, and absorption is restricted to the values of about 10^3 cm^{-1}.[3,26]

View Article Online
DOI: 10.1039/C8CP06209A

In our previous work, it was discovered that polarization of the emitting light from $TlGaSe_2$ is out-of-layer plane, suggesting the *e-h* emitting dipoles (excitons) are orthogonal to the crystal layer.[7] Furthermore, we obtained that in $TlInS_2$ the excitonic PL exhibit a large Stokes shift from the direct exciton absorption.[24] Also, we detected enhancement of the PL intrinsic intensity in $TlInS_2$ crystals with small additions of B, Ag and Er dopants. The most pronounced enhancement was discovered in crystals doped by *Erbium*.[24] This result is unexpected, since extrinsic impurity in ionic semiconductors usually reduces the intrinsic radiation due to charge trapping.[27]

In the current work, we provide comprehensive study of the charge carrier dynamics in $TlInS_2$ crystals after short laser pulses under diverse excitation conditions. The paper is organized as follows.

After giving experimental details (Sec. 2 and Supplementary file), in Sec. 3.1 we examine time-resolved PL under a single-photon (SP) and a two-photon (TP) generation. The results confirm intrinsic excitonic radiation analogous to the steady-state PL (SPL), and show insignificant bandgap shift with excitation level. The PL enhancement in the Er-doped $TlInS_2$ crystals is established to be a result of longer radiative lifetime in spite of considerable decrease of nonradiative lifetime. The exciton out-of-plain polarized dipoles occur instantly at any excitation level. A distortion of them however can take place in less of 10 ps-time as found in the undoped $TlInS_2$. This behavior implies presence of genuine defects, which we assign to the PSFs that are able to destroy oscillator strength of polarized excitons.

In Sec. 3.2 and Sec 3.3 we examine injection dependences of nonradiative lifetimes and the carrier diffusion using the transient grating (TG) and the pump-probe (PP) techniques. Inverse correlation is observed between mentioned parameters suggesting a coupled in-plain *e-h* transport to a single recombination sink. However we show that behavior of the undoped and the Er-doped $TlInS_2$ crystals are quite different. In both cases, the dynamics do not exhibit nonlinear Auger recombination and do not show ambipolar diffusivity reduction caused by the band-gap narrowing (BGN) at high excitations. The absence of these phenomena suggests a spatial separation of excess pairs.

In Sec. 3.4 we describe measurements under intense power pulses. Above the critical intensity, the TG light produces remarkable optical imprints in $TlInS_2$ samples in a form of fringes. These imprints are metastable but revert to permanent ones at higher intensities. The micro-Raman and micro-PL scans indicate appearance of new crystal phases in fringes. We assign the formation of these phase by giant Stark effect produced due to separation of *e-h* charges. For the best of our knowledge such experimental result has not been reported up to date.

The Sec. 4 is devoted to comprehensive discussion. We present the universal model of the spontaneous 2D-layered crystal polarization which explains versatile results. We assume that boundaries of the PSFs act as the most prominent linear recombination sink. The frequency of the PSF distribution in depth is taken to provide intricate difference between the undoped and the Er-doped $TlInS_2$ crystals. Numerical modeling of the carriers diffusion and recombination along layers allowed to evaluate their diffusion lengths that was found to be comparable with a mean PSF sizes (SI. 4). The model of the spontaneous 2D-layered crystal polarization is consistent with reported phenomena of external transverse electric fields in 2D-layered chalcogenides.

Then, in the conclusion we summarize our main results.

2. Samples and experimental details

The crystals were grown by modified Bridgman method in evacuated to pressure of 10^{-5} Torr silica tubes using high purity components taken in stoichiometric proportions. The incorporation of *Erbium* was produced by adding it in amount of molar concentration of 0.2 % in the melt. The slices of samples of a few millimeters sizes and hundred micrometers thickness with high surface quality were prepared by cleaving crystal along the layers. Both crystals (pristine and with *Er*) were yellow in color and demonstrated a sharp drop in optical transparency at the indirect gap threshold.[24] By the energy-dispersive X-ray analysis, we determined the same ratio of the main elements (Tl, In, Se) in both type of the samples. The micro-Raman spectra recorded with Nanofinder-HE apparatus are shown in Supplementary file (Fig. S2). Those are identical in both crystals, in good agreement with previously published Raman spectra.[28,29] This

View Article Online
DOI: 10.1039/C8CP06209A

result gives strong evidence that amount of *Erbium* introduced in $TlInS_2$ does not provide noticeable substitution on a layer atomic structure.

For transient PL measurement, the 160 fs duration pulses from optical parametric amplifier pumped by *Pharos* laser were used as an excitation source. The laser was operating at 10 kHz repetition rate with ~1% energy stability and the pulse energy was controlled by ND filter. The beam was tilted 15 degrees with respect to c-axis. The excitation spot on the sample surface was about 90 μm in diameter as was measured with knife edge at 1/e of intensity. Two s-polarized excitation wavelengths of 460 nm and 680 nm have been employed in the study. The 460 nm excitation has energy above E_g^d and provides a SP generation at penetration depth of 5 μm.[3] The 680 nm excitation provides TP absorption. The PL emission was collected in backward direction within 25 degrees angle. The *Acton* spectrophotometer equipped with *Hamamatsu* streak camera was used for emission analysis. The dynamic range within five orders of magnitude was obtained by regulating gain on a multi-channel plate. The time- and spectral-resolution of PL record is 10 ps and 10 meV, accordingly. An averaging of 100 sequences for single spectrum recording was used.

The TG investigation was conducted according to the scheme shown in Fig. 2. The excitation was carried out by Nd:YLF *Ekspla* laser with 7 ps pulse duration at the second harmonic 527 nm wavelength with 10 Hz repetition rate. The pulse energy was attenuated by half-wave plate and a *Glan* prism. The holographic beam splitter of two coherent beams and two focal lenses (f_1, f_2) were employed to adjust a 100% contrast in the interference grid-pattern. The excitation spot was 320 μm in diameter. The spacing period Λ was varied over 1-8 μm range. The probe pulse at 1.053 μm wavelength was delayed by 30 cm optical line (with a quadruple beam pass) and projected into the center of the excited spot. The transmitted, I_T, and the diffracted, I_D, beams were detected by 16 bit *CAN* detectors. The compression of the noise was achieved using normalization of the diffracted beam to the transmitted one under the 5% tolerance interval for the excitation pulse energy.

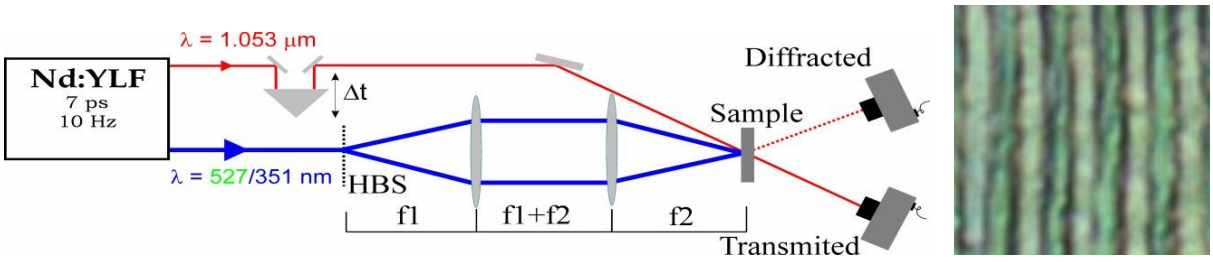

Fig. 2. (left) The schematic diagram of the TG recording. The sample is excited by two well overlapping 527 nm interfering light pulses. The corresponding diffraction pattern is monitored by delayed probe pulse at 1.053 μm wavelength, see details in,[29]); (right) Imprinted optical pattern at 15mJ/cm^2 fluence in the undoped $TlInS_2$ crystal with Λ = 2.1 μm spacing; Nomarsky microscope image measures 10×10 μm^2.

The carrier concentration induced by the interference pattern can be expressed as $\Delta N_{(t=0)}(1 + \cos(2\pi x/\Lambda))\times\exp(-\alpha z)$ where x is a coordinate in the grating vector direction and $\Delta N_{(\Delta t=0)}$ is the maximum of the excited carriers at the initial time of overlapping pump-probe pulses. $\Delta N_{(\Delta t=0)}$ is proportional to the incoming pump intensity I_{inc}, namely, $\Delta N_{(\Delta t=0)} = (1-R)\alpha I_{inc}/h\nu$. Here $\alpha \cong 100$ cm^{-1} is the absorption coefficient, $R = 0.20$ is the optical reflection coefficient at $h\nu = 2.35$ eV.[26] The excited carriers induce change in the complex refractive index of the material which can be described by the classical Drude-Lorentz model. Customarily, diffraction occurs due to the change in the real part of the refractive index, Δn_{FC}, which is proportional to the ΔN with coefficient n_{eh} counted for a single *e-h* pair.[31] In the most semiconductors, n_{eh} is of order 10^{-22} cm^3.[32] The TG erasure is monitored by tracing time-dependence of diffraction efficiency: $DE(t) = I_D(t)/I_T(t)$ which quantitatively represents square of change of refractive index. Assuming an exponential decomposition in parameters the DE assumes the following form [33]:

View Article Online
DOI: 10.1039/C8CP06209A

$$DE(t) = \left(\frac{\pi n_{eh} \Delta N_{(t=0)}}{\alpha \lambda} \right)^2 \exp\left(-\frac{2t}{\tau_G} \right), \quad (1)$$

$$\frac{1}{\tau_G} = \frac{1}{\tau} + \frac{4\pi^2 D}{\Lambda^2}. \quad (2)$$

where τ_G τ and D are the grating erasure time, the nonradiative recombination lifetime and the diffusion coefficient, respectively. The individual values of τ and D could be obtained from measurements at different Λ.[34] (Note that diffusion occurs between fringes along the layers.) In our experiment, the excess carrier concentration was varied in the range of 10^{16}-10^{19} cm^{-3}, which by 3-6 orders of magnitude exceeds the equilibrium carrier concentration. Thus, the ambipolar diffusion coefficient for equal concentration of excess *e-h* pairs can be expressed by the following formula [35]:

$$D = 2D_eD_h/(D_e + D_h), \qquad D_e = (kT/q)\mu_e, \quad D_h = (kT/q)\mu_h \quad (3)$$

where q is electron charge, D_e and μ_e, as well as D_h and μ_h are the diffusivity and mobility of electron and hole connected by Einstein relation.

The pump-probe (PP) measurements were carried out under perpendicular geometry of excitation and probe beams using the free–carrier-absorption (FCA) technique.[36] The excitation laser generated pulses of 2 ns duration at 525 nm wavelength and was operating at 40 Hz repetition rate. The probing beam was provided by tightly focused light from 1.3 μm cw-LED. The PP transients were recorded by 0.5 ns risetime InGaAs photoreceiver with subsequent averaging of 10^3 signals and the data processing by a digital 1 GHz bandwidth oscilloscope. The FCA cross-section of 5×10^{-18} cm^2 at the probe wavelength was used for signal conversion into the excess carrier concentration. The probing was performed at a depth of 50 μm below of the excited surface, see details in Ref. [21]. All following time-resolved studies were performed at RT.

3. Results

3.1 PL spectra and radiative decay

The integrated PL spectra in investigated crystals are presented in Fig. 3. The spectra shape and PL peak position are similar in appearance for both SP and TP generation cases. However, TPA affords higher emission intensity accumulated from large crystal volume. In both cases, no PL peaks shift is observed but PL band broaden up to 30-40 meV with increasing pulse fluence. In Fig. 3 a,c, for comparison, we inset two previous spectra obtained by the SPL shown here by blue dots as measured in the same crystals.[24] The SPL spectra are in good agreement with time-integrated PL. The PL peak fluctuation of 0.02 eV occurs on different sample spots, as was noted before.[24]

View Article Online
DOI: 10.1039/C8CP06209A

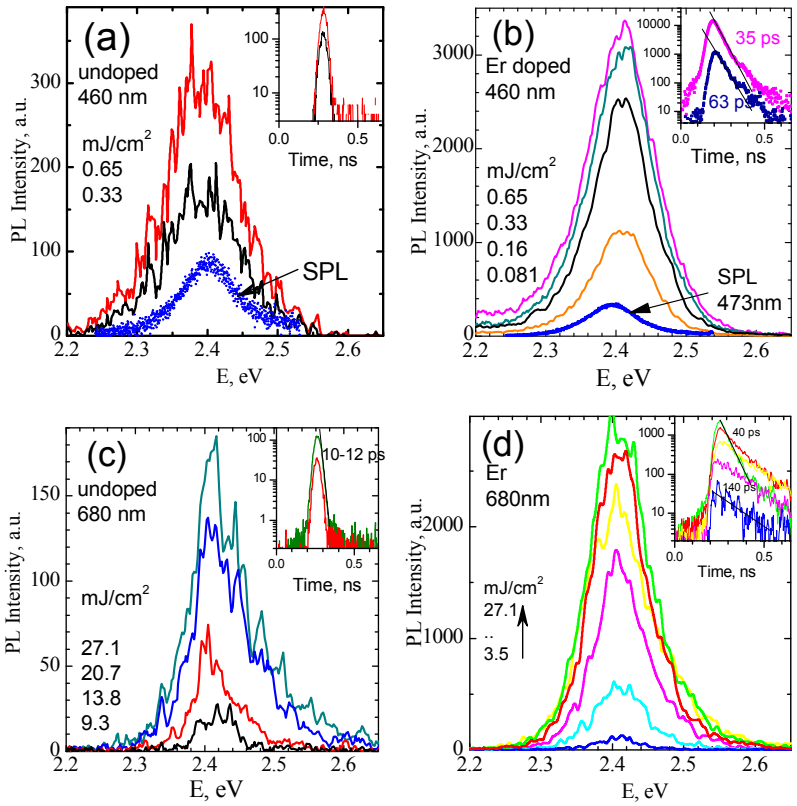

Fig. 3. Time-integrated PL spectra of undoped and *Erbium* doped $TlInS_2$ crystals excited by fs-pulses with different energy for SP generation at 460 nm (a,b) and TPA at 680 nm (c,d). Two spectra of steady-state SPL [24] are included in (a,b) panels for comparison. The inserts show PL transients at a few excitation fluences.

By comparing emission intensities we detect a strong enhancement of the PL efficiency in the *Erbium* doped $TlInS_2$ crystal for both types of generations. The enhancement is clearly seen by congruence of numbers on the ordinate scales (Fig. 3) where intensity is shown in arbitrary but the same units. However, precise enhancement cannot be determined for a reason of large inhomogeneity in emission from different spots on each sample. We estimate the enhancement to be within factor 50 on average. The PL peak dependences from the most favorable emitting spots in each sample are shown in the Figure 4 a,b as a function of the excited pulse fluence. The fit of PL intensity dependence with a slope 1.0 (solid line) corresponds a direct proportion of it to the excitation fluence for SP generation while the slope of the fit for the TPA is equal to 2.0.

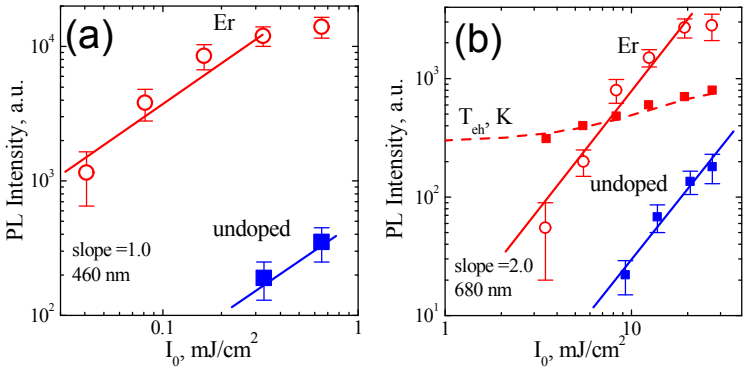

Fig. 4. Time-integrated PL intensity in undoped (solid symbols) and *Er* doped $TlInS_2$ crystal (open symbols) *vs* excited pulse fluence on the most favorable emitting spots for SP generation (a) and TPA (b). The slope of the

View Article Online
DOI: 10.1039/C8CP06209A

dependence is approximated by solid lines in a double log-scale. Statistical variation is shown by arrows. Solid squares and dashed line in (b) show *e-h* gas temperature.

In view of all discovered facts, we identify that time-resolved PL has common origin with the SPL. In Fig. 5 we present the SPL peak variation with temperature in undoped (open circle) and *Erbium* doped (open diamonds) $TlInS_2$ crystals. Here on the left and right axes we present two *Er*-doped sample at 24 K and RT, respectively. The PL band width (at 1/e level) decreases from 120 meV at RT down to 30 meV at 24 K. For comparison, the appropriate values of the indirect band gap $E^i_G(T)$ [26] and position of the direct exciton peak E^d_x temperature variations from literature [24] are included in the plot. In both crystal types, the PL peak has identical Stokes shift from E^d_x. The largest shift of 80 meV occurs in I-phase around 200 K. The analysis of PL fine structure at low temperature allows concluding that LO phonon assistance can explain only a quarter of the Stokes shift. Therefore, it can be assumed that the rest of PL energy shift occurs for exciton out-of-layer transformation as was originally noted in [24].

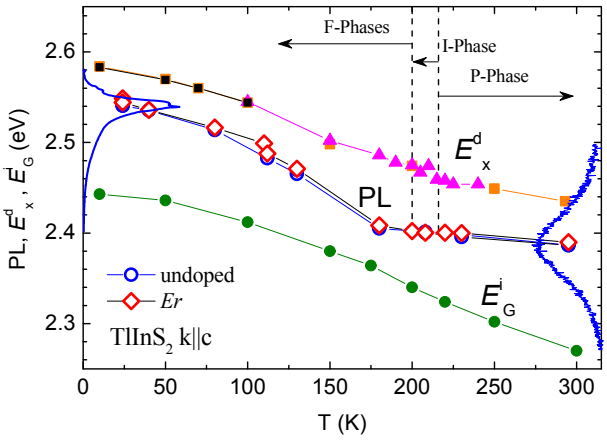

Fig. 5. SPL peak *vs* temperature in undoped and *Erbium* doped $TlInS_2$ crystal together with variation of the direct exciton position E_x^d and the indirect band gap E_g^i (taken from various literature sources [24]). Crystal phase regions are indicated. Two SPL spectra of *Er* doped $TlInS_2$ at 295 K and 24 K are exposed.

Time-resolved measurements for *Erbium* doped $TlInS_2$ crystal at RT show that PL of all emitting wavelengths has identical radiative transients as illustrated in Fig. S4. Some integrated PL decays are shown in the insets to Fig. 3. In the $TlInS_2$(Er) crystal, the transients are located on a sub-nanosecond time scale. The most unexpected feature is that for the undoped crystal the radiative lifetimes are very short (Fig. 3 a,c) in a clear contrast to the long nonradiative lifetime, see section 3.2.

Using measured TP absorption coefficient β = 10 cm/GW in the $TlInS_2$,[37] we estimate the emission from hundred to ten micrometers depth for used excitation pulse fluences 4-20 mJ/cm^2. The relaxation of hot carriers occurs in less than one picosecond by a cascade emission of longitudinal optical (LO) phonons. This evolution becomes possible since the excess energy after TP absorption is 1.2 eV above the band gap, much larger than the energy of LO phonon.[28] If the characteristic temperature of the thermalized carriers has not reached the lattice temperature, the *e-h* plasma temperature will be reflected on the high-energy tail in the spectra which may be depicted by the following expression [38]:

$$I(h\nu) \propto \exp[-(h\nu - E_g^d)/kT_{eh}] \qquad (4)$$

where T_{eh} is plasma temperature. The PL higher energy tails of $TlInS_2$(Er) crystal are shown in Fig. S3 b and the extracted T_{eh} values are represented in Fig. 4 b. It is clear that below 4 mJ/cm^2 the carrier heating is negligible and their temperature does not differ from the lattice temperature. The maximal T_{eh} exceeds 800±50 K for excitation fluence above 20 mJ/cm^2 where the energy of hot carriers reaches LO phonon

View Article Online
DOI: 10.1039/C8CP06209A

energy. The heating in *e-h* plasma explains why radiative lifetime is decreasing with increasing excitation and also why PL intensity saturated at high fluence.

3.2 TG and PP investigations of nonradiative lifetime and diffusion

Figure 6 shows examples of the results obtained by TG measurements. A plot of DE magnitude at $\Delta t = 0$ in Fig. 6 a obeys the quadratic dependence on the excitation fluence.[30] According to Eq. (1) it testifies that excess electron concentration increases linearly with excited photons, i.e. $\Delta N_{(\Delta t=0)} \sim \alpha I_{inc}$ as expected for SP generation to the bottom of the indirect band gap. The normalized TG decays for two Λ periods are shown in Fig. 6 b,c. In the case of Λ_2 = 2.1 μm the τ_g differs little from recombination lifetime since influence of the second term in Eq. (2) is less than 20%. For the Λ_1 = 1.1 μm the decay becomes faster because of augmentation in diffusion flow by a factor of $(\Lambda_2/\Lambda_1)^2$. These decays indicate major difference observed in the two crystal types. In the $TlInS_2$(Er), the DE decay is exponential in three orders of magnitude and similar diffusion influence is evident from decay constants between Λ_2 and Λ_1. By contrast, in the undoped $TlInS_2$, the exponential relaxation is observed only within the first 200 ps (Fig. 6 b) and by a constant impact of diffusion. After 200 ps, a slower non-exponential decay with instantaneous lifetime $\tau_{inst} = -2DE(t)/(\delta DE(t)/\delta t)$ is evidenced and the role of diffusion is clearly decreasing. In Supplementary file (Fig. S4) transients at different fluences in undoped $TlInS_2$ are shown.

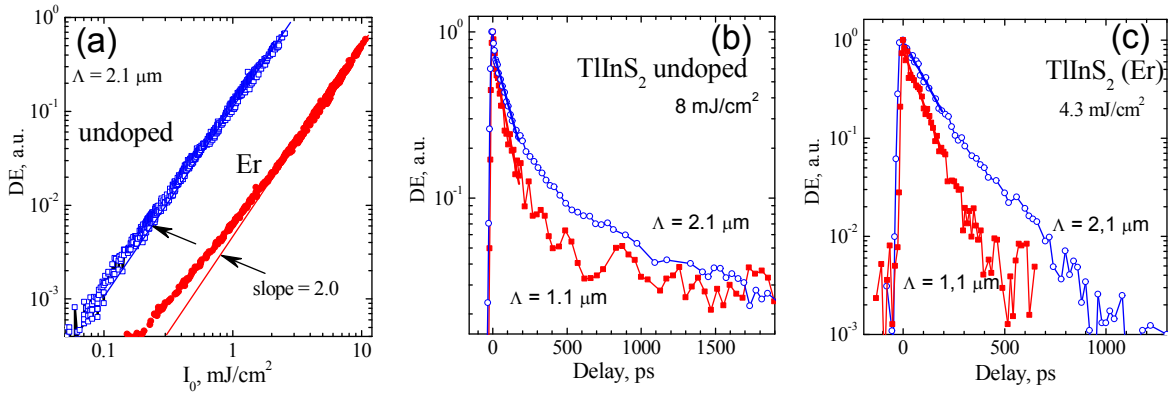

Fig. 6. (a) Diffraction efficiency magnitude of TG ($\Delta t = 0$) versus the intensity of 527 nm pump. The data for the *Erbium* doped sample are lowered by one order to enhance clarity of the figure. The slope 2.0 is indicated by solid lines. The normalized grating decay kinetics at two periods Λ_1 and Λ_2 in the undoped (b) and *Erbium* doped $TlInS_2$ (c).

To facilitate more strict quantitative comparison, the grating decay time τ_G was obtained from the initial exponential path of the DE as indicated by straight lines (Fig. 6 b,c). Then, the bipolar diffusion coefficient D and the nonradiative lifetime τ were determined from the slope and the intersect with ordinate axis of relationship between reciprocal τ_G and reciprocal Λ^2. The extracted data are presented in Fig. 7. The solid symbols expose inherent spread of parameters on surface spots of undoped $TlInS_2$. Data variation was essentially smaller in the *Erbium* doped crystals; therefore they are represented by a single open square symbol. The applied lines in Fig. 7 are guides to the eye. The diffusivity and lifetime vary only slightly in $TlInS_2$(Er) while in the undoped $TlInS_2$, lifetime strongly decreases and the D values increase with excitation level. However, in both crystals an inverse variation between τ and D is clearly observed. At the highest excitation, very similar values of τ = 0.3 ns and $D \geq 1$ cm^2/s are attained.

View Article Online
DOI: 10.1039/C8CP06209A

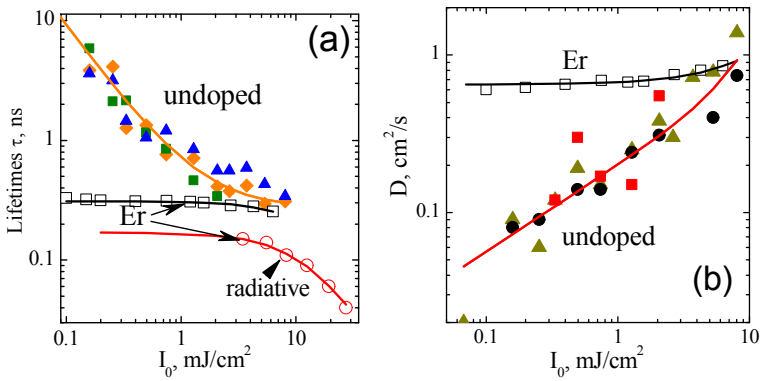

Fig. 7. Nonradiative lifetimes (a) and diffusion coefficient (b) obtained by TG measurement as a function of excitation pulse fluence in undoped (solid symbols) and in Er doped $TlInS_2$ (open squares). The radiative lifetime in (a) is shown by open circles.

In Fig. 7 a we include radiative lifetime in *Erbium* doped $TlInS_2$ (open circles) where x-scale is adjusted for TP generation, see also Fig. S6. These data indicate that radiative decay is twice faster than the nonradiative one. Such property is expected for typical bimolecular kinetics where emission intensity is ruled by two equal electron and hole concentrations $\Delta N = \Delta P$, e.g. $I_{PL}(t) = \beta \Delta N(t) \Delta P(t)$.[39] This relationship is established only for the $TlInS_2$(Er) crystal. In the undoped crystal, as noted before, the radiative lifetime is much shorter than the nonradiative one.

The entire picture of nonradiative decays is shown in Fig. 8 over eight time orders. The excess carrier concentration $\Delta N(t)$ was calculated from assembled TG transient (two excitation intensities, solid symbols) and with PP transient (single intensity, open symbols). The numerical fitting is presented by lines using a criterion of minimal number of used components. Overall conformity is given by green solid line and matching lifetimes are listed in Table 1. A slow relaxation in the undoped crystal fits by two exponents which saturate with increasing excitation at $\Delta N_1 = 1.2 \cdot 10^{15}$ cm^{-3} and $\Delta N_2 = 3 \cdot 10^{15}$ cm^{-3}, respectively. These values are similar to ones identified in $TlGaSe_2$ at RT in Ref. [21], namely, $\tau_1 = 400$ μs, $\Delta N_1 = 7 \cdot 10^{14}$ cm^{-3}, and $\tau_2 = 4$ μs, $\Delta N_2 = 4 \cdot 10^{15}$ cm^{-3}. (Slow lifetimes in $TlGaSe_2$ were increased by orders of magnitude with decreasing temperature). We believe that these slow components in both layered semiconductors have origin of slow carrier capture by deep traps, detected by PICTS technique.[11]

The third component (Table 1) contributes relaxation in time range from nano-to-microseconds. It reveals itself in the undoped $TlInS_2$ at carrier densities $5 \cdot 10^{15}$ - $2 \cdot 10^{17}$ cm^{-3}. The component can be described by a stretched exponential function (red line) with lifetime $\tau_3 = 5$ ns:

$$\Delta N(t) = N_3 \cdot \exp(-t/\tau_3)^{\beta} \qquad (5)$$

where $N_3 = 2.3 \cdot 10^{17}$ cm^{-3} and the dispersion factor $\beta = 0.42$. The dispersion determines curvature of the decay of single independent exponentials distributions. Both τ_3 and β parameters are slightly dependent on the excitation level. The three mentioned components well represent the overall decay below $\Delta N(t) = 3 \cdot 10^{17}$ cm^{-3}. Several models explaining the physical origin of stretched exponential line have been put forward for recombination decay in disordered semiconductors.[40] Our present data (see discussion below) are in favor of a model that the component is a consequence of the carrier temporal localization for their transport along the layer. Thus, we need an explanation why such localization is well expressed in undoped $TlInS_2$ crystal. The fourth component is described by exponential function with a constant lifetime of $\tau_4 = 0.3$ ns. It reveals at higher excitation in both crystals and has nonsaturable magnitude. For *Erbium* crystal, this component alone extends below 10^{16} cm^{-3}.

View Article Online
DOI: 10.1039/C8CP06209A

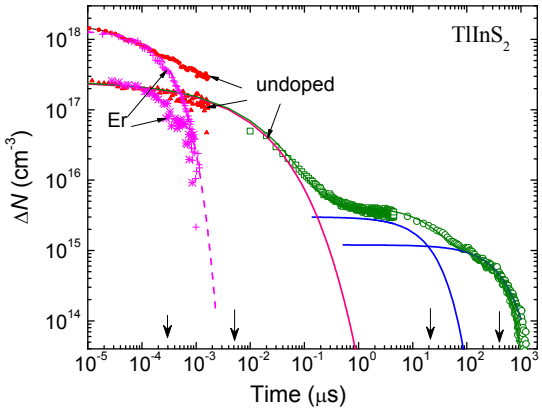

Fig. 8. The decays of excess carrier concentration in $TlInS_2$ crystals on a log-log time scale. Open symbols represent data from the PP and crosses from the TG measurement. The overall fit for undoped crystal is given by a green solid curve in which consists of components shown by blue lines and a stretched exponent (red line). Magenta crosses represent data for *Erbium* doped crystal (TG measurement). The lifetime of 0.3 ns appears as dashed-magenta line. Vertical arrows indicate characteristic lifetimes, see Table 1.

TABLE 1. The characteristic parameters of the decay in $TlInS_2$ crystals.

Component	Lifetime	Magnitude
1 Exponent	τ_1= 410 μs	Saturated at $1.2\cdot10^{15}$ cm^{-3}
2 Exponent	τ_2 =20 μs	Saturated at $3\cdot10^{15}$ cm^{-3}
3 Stretched exponent	τ_3 = 5 ns, β = 0.42	Above $5\cdot10^{15}$ cm^{-3}, partially saturated
4 Exponent	τ_4 = 0.3 ns	Unsaturated

3.3 Absence of non-linear Auger recombination and band gap narrowing (BGN)

It is significant to point out that lifetimes and diffusion behavior in layered crystal is in a contrast with those of isotropic indirect-gap semiconductors. In crystalline Si, SiC and GaP,[44] approaching high injection regime, carrier lifetimes strongly decreases due to non-linear Auger recombination process. This fact simply implies that, in dense plasma of fermions, the energy transfer between the bipolar particles can occur easily. The Auger rate can be presented by inverse recombination lifetime $1/\tau_A = \gamma\Delta N^2$ where Auger coefficient γ describes probability of a third particle accepting energy from annihilating *e-h* pair. The excitonic interaction yields an increment of γ values even above the excitonic Mott transition.[45] However, above mentioned figures do not confirm contribution of the Auger recombination in layered $TlInS_2$ (Fig. 7 and Fig. 8). The same was noted in $TlGaSe_2$.[21]

The ambipolar diffusion coefficient *D* in isotropic 3D semiconductors gradually decreases with excitation above 10^{17} cm^{-3}. This feature is triggered by BGN effect, a phenomenon confirmed in Si,[35] SiC [46] and diamond.[47] Ambipolar diffusion occurs against a gap gradient by occurrence of negative ΔE_g which increases with excess concentration. Theoretically BGN has been explained taking into consideration the interaction of electronic self-energies (exchange and correlation) of individual fermions in uniform dielectric medium.[48] The calculation assumes density repulsion according to the Pauli principle which leads to redistribution in energy system in such a way that in vicinity of particular hole electrons are found with higher probability than other holes and *vice versa,* increasing particle correlation. The approach allows setting quasi-Fermi thermodynamic levels for electron and hole system. Absences of *D* reduction in the layered crystals imply that *e-h* pairs are separated in a real space and their wavefunction overlapping is small.

View Article Online
DOI: 10.1039/C8CP06209A

3.4 Optical imprints under intense laser pulses

The electronic character of transients in both types of $TlInS_2$ crystals after 527 nm pump was established for laser pulse fluence up to 10 mJ/cm^2. However, above this value, some metastable and permanent transformations were discovered. All changes occurred below an optical breakdown which was estimated experimentally to be 50±15 mJ/cm^2. In the current section, we present illustration of the results in the fluence range 10-30 mJ/cm^2. In such study we have employed the following procedure. First, a fresh area of crystal was excited by TG interference pattern in time interval of 0.5-2 seconds with a frequency of 10 Hz. Then, the pump beam was closed by a shutter, and the diffraction dynamics was monitored in the crystal by probe beam. Or, in some instances, the procedure of pumping and probing cycles without pump was repeated.

Fig. 9 a shows transient in $TlInS_2$ crystals after exciting with pulses of 10-12 mJ/cm^2 over the course of 2 s. The DE kinetics reveals reset with exponent of 12 seconds slope quite identical in both $TlInS_2$ crystal types. At the end of reset, DE reaches the background level. We should note that background signal is present always in TG measurement because a probe light is scattered in the sample. The scattering can be reduced somewhat by aperture placed before a detector. Other reductions of noise-to-signal also can be achieved, see details in [41]. Note, that the scattered light is higher in layered crystals due to disordered interfaces.[24] The observed DE reset in Fig. 9 a, clearly cannot be attributed to the thermal grating since the lattice thermal grating diffusivity can be accounted by the formula $D_T = \varkappa/\rho C_p$ where $\varkappa$ is thermal conductivity, ρ is the mass density and C_p is the thermal capacity. We expect that thermal lattice grating lifetime for Λ = 1 μm period should be in the range of 1-10 ms,[41] much shorter to that observed in Fig. 9 a. We hypothesized that crystal structure of $TlInS_2$ is subject to metastable transformation set by intense TG fringes. We have observed that metastable state transforms into a permanent one when excitation fluence exceeds 15 mJ/cm^2. Examples of the imprinted fringes observed by Nomarsky microscope are shown on top of Fig. 9.

Figure 9 b demonstrates DE evolutions after repetitive 0.5 s excitation cycles at 28 mJ/cm^2. The excitation starts at t = 0 and the probing is achieved in 2 s interrupting cycles. The electronic TG component is hidden due to a used long time scale. Instead, it is obvious that DE background sufficiently increases by first cycles as indicated by a dashed line. Then, the background saturates at t = 20 s and drops a little in continuation.

Another temporal variation of the DE background as produced by pulses with 21 mJ/cm^2 sequences is shown in Fig. 9 c. Here, only the signal associated with probe background is presented. In this plot, for a reference, we perform a measurement on 500 μm thick double side polished Si wafer. The initial background on Si wafer is very low, about three orders of magnitude below that in $TlInS_2$ owing to perfection in polished wafer surfaces. One can see that background in Si rapidly rises by excitations and steeply drops at t = 22 s. The surface inspection performed by micro-Raman shows that amorphous phase is formed in the bright fringe in Si. After following excitation cycle, the amorphous phase spreads along all the spot and the contrast between bright and dark fringes decreases suddenly. Notice that 527 nm laser light is efficiently transferred to Si crystal lattice because its quanta energy of 2.35 eV is much above the indirect band gap of 1.2 eV. Si melting occurs as a result of a strong band-to-band absorption with coefficient > 10^4 cm^{-1} in a micrometer-depth.[42] The numerical calculation shows that excess carrier concentration reaches values above 10^{21} cm^{-3} and Si melting temperature of 1450° C is exceeded.[43] In $TlInS_2$, in contrast the quantum energy above the band gap is small (~0.02 eV); the absorption is a bulk-like and the excess carrier density is at 2-3 orders lower than in Si. From Fig. 9 c we see that new crystal phase stabilize its structure and $TlInS_2$ crystal exhibits resistance to the following modification.

View Article Online
DOI: 10.1039/C8CP06209A

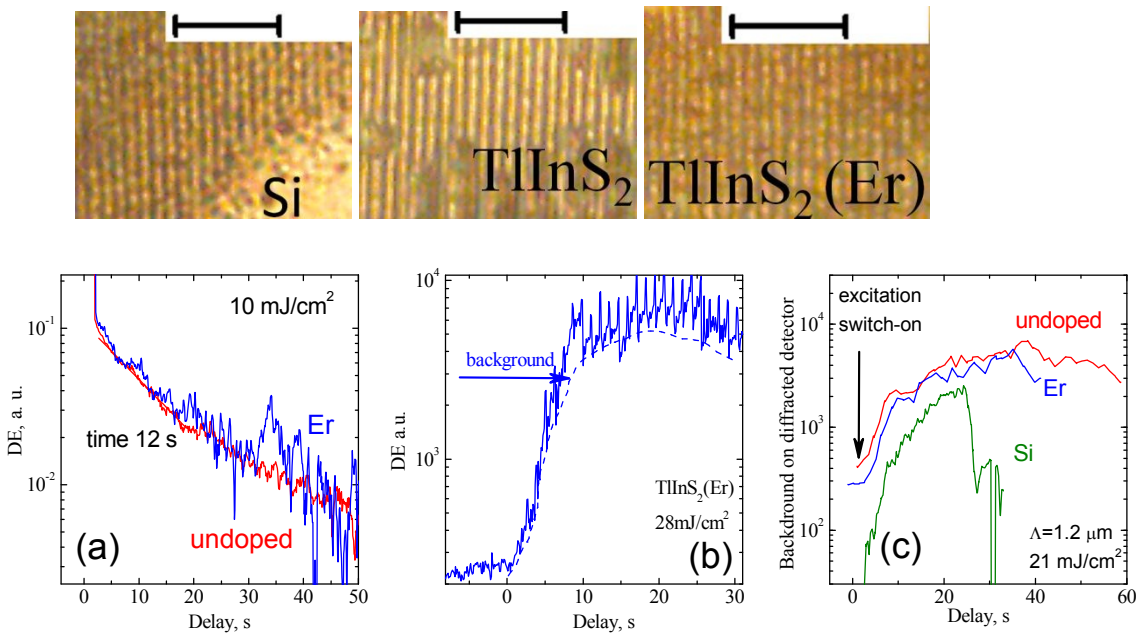

Fig. 9. Top panel: examples of imprinted fringes on Si wafer, $TlInS_2$ and $TlInS_2$(Er) after excitation with fluences about 20 mJ/cm^2, Λ = 1.1 μm, scale bar 10 μm. Bottom: (a) Metastable DE reset in $TlInS_2$ and $TlInS_2$(Er) samples after 15 mJ/cm^2 pulses within 2 s. (b) DE background signal (dashed line) at 28 mJ/cm^2 in $TlInS_2$ with a 0.5 s irradiation and 2 s interaption probing sequences. (c) The dynamics of the background on a longer time scale in Si and in two types of $TlInS_2$ crystals at 21 mJ/cm^2 fluence.

In other experiment, the light imprinted fringes were obtained by larger TG period, as shown in Fig. 2 (Λ =2.1 μm) and in Fig. 10 (Λ = 8 μm). The images are permanent and stable within weeks.

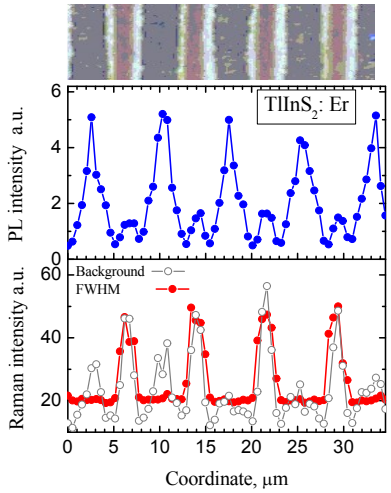

Fig. 10. Light imprinted optical pattern with TG period Λ = 8 μm in $TlInS_2$(Er), and the scanning of integrated SPL (filled blue circles) and the Raman scattering: Background – in the range of 180-240 cm^{-1} (open circles), FWHM of the main line doublets at 285 cm^{-1} (filled red circles). The measurement is produced with 473 nm wavelength.

The inspection of them has been performed using micro Raman scattering (see Suppl. SI. 1) and micro-SPL integrated over 2.3-2.53 eV range. The scanning results are presented in Fig. 10 and show correlation to the imprinted image pattern.

View Article Online
DOI: 10.1039/C8CP06209A

Examining these results, we have found five times large SPL in the places of a new phase and some increase of Raman background intensity. However there is another set of smaller SPL in about 2 times distribution with a larger Raman background intensity and increase of the FWHM on the main Raman doublet lines centered at 285 cm^{-1}. Such different alternation is implying that two different crystal phases are created with larger periodicity than TG period. This fact suggests that crystal parameters can be changed by phase transformation like the extinction coefficient ***k,*** the refractive index ***n*** in according with strength of the intrinsic oscillator exciton emission. We assign the formation of new crystal phases with interior Stark electric field created perpendicular to the layer which produces arrangement in interlayer atom structure. As far as we know, such light-induced effect for the first time is described here for the first time. More investigations clearly are needed for understanding the stability and mechanism of the light imprint fringes in $TlInS_2$ crystals.

4. Discussion

4.1 Main experimental observations in layered crystals: Important similarities and differences

Generally, quite long time relaxation of excess pairs exists in both $TlInS_2$ and $TlGaSe_2$ layered crystals and both compounds show SPL anisotropy in respect of excitation directed to the layer plane and of PL out-of-plain polarization.[21] This suggests that radiative recombination is qualitatively similar due to their layered structure. The SPL emission in $TlGaSe_2$, however, is sufficiently lower and the crystal has much higher anisotropy of resistivity in perpendicular and parallel to the layer.[2,7]

Another distinctive feature of layered ternary crystals is absence of surface related carrier recombination despite of a long carrier decays. The surface recombination creates profiles of the carrier diffusing toward surfaces pronounced in Si and SiC,[44,49] but those are not observed in $TlGaSe_2$ and $TlInS_2$.[21] We provide evaluation of this phenomena using mobility in $TlInS_2$ from Hall effect measurement by Gasanly et al.[50] At RT mobility of electrons and holes parallel to the layers was found to be $\mu_{e\|} = 37$ cm^2/Vs and $\mu_{h\|} = 23$ cm^2/Vs, respectively.[50] Using Einstein relation (Eq. 3) we evaluate the ambipolar diffusivity as $D_{\|} = 0.74$ cm^2/s. On the other hand, using the resistivity ratio across/along layers in $TlInS_2$ (in order of 10^{-3} [1,2]) the diffusivity perpendicular to the layer can be reduced by this factor and reach value of $D_{\perp} \leq 7.4\ 10^{-4}$ cm^2/s . This low magnitude is in agreement with absence of surface recombination. The value $D_{\|}$ is comparable with our results presented in Fig. 7 b showing that the diffusion along the layer dominates.

In the present work we found drastic PL enhancement in *Erbium* doped $TlInS_2$, crystal in which the nonradiative lifetime is shorter and the ambipolar diffusivity is higher compared to that in undoped $TlInS_2$. It means that recombination described by stretched exponent in the undoped $TlInS_2$ does not involve in creation of radiative dipoles. On the other hand, both crystal types have similar lifetime at high excitation level $\tau_4 = 0.3$ ns and similar diffusivity while the radiation efficiency is the same as for low excitation. This might be caused by out-of-layer exciton separation and distortion within first picoseconds. This effect happens at any excitation level. Thus, we are now in a position to discuss the model which can provide explanation for these discriminating findings. The model should explain: (i) the light induced crystal phase transformation, (ii) absence of Auger recombination and the BGN effect, and (iii) should be consistent with reported giant Stark effects in the transversal electric field. At the same time, the model has to provide an explanation for PL enhancement in *Erbium* crystal while the temperature dependence of the SPL energy peak in both crystal types is the same (Fig. 5).

4.2 Model of spontaneously polarized layered crystal

Based on 2 times large linear expansion coefficients ($\alpha_{\|} < \alpha_{\perp}$) reported for $TlInS_2$ and $TlGaSe_2$,[51] we propose that atomic bonds in layer plane have a mismatching with interlayer bonds. This property allows us associate a layer structure with a condenser, i.e. a pair of closely placed infinite plates where a charge transfer between planes may take place. The freedom to transfer charge between

View Article Online
DOI: 10.1039/C8CP06209A

set of two layers introduces the spontaneous polarization. This feature is used to reduce total energy in layered crystal and is the reason why ternary dichalcogenides have easy ability of phase transition at low temperatures and poling by external transverse electric field. The electric dipole moments associated with spontaneous polarization are essentially localized on each layer pair. If closely placed condensers are becoming charged in serial, in a crystal of finite dimensions the spontaneous polarization would lead to a huge potential difference across the crystal in c-direction. To avoid electrical field buildup by electric dipole moments, there must be macroscopic depolarization field in the opposite direction.[52] A depolarization field arises in real crystal from: (i) the accumulation of the surface charge, (ii) certain distribution of free carriers in the bulk, and (iii) from polarization of extrinsic dopants, like defect-density-waves.[15,16] Also screening by polarization of valence band electrons may take place. The presence of depolarization field explains why ternary dichalcogenides always behave as self-compensated and isolated semiconductors.[1]

The combination of spontaneous polarization with a constant depolarization field should lead to the 'sawtooth' potential of zigzag pattern as shown schematically in Figure 11 a. Due to interlayer bonds,[11-13] this potential is felt by electron transition in the c-direction in the perfect crystal. The portion of potential with a positive slope represents the steps associated with spontaneous polarization, whereas the portion from the depolarization field having a negatively slope represents potential from constant depolarization field. The height of the potential step in dipole can be, to very crude estimation, of a few meV. In Fig. 11 b we show a combination of such potentials in the crystal which contain double PSF. We suggest that double PSF are common since the system in this case can gain additional crystal energy by a small distortion of the interlayer bond length. While other PSF shapes may take place, we avoid discussing them for simplicity. As can be seen from Fig. 11 b, the PSF presence sufficiently changes polarization and depolarization field in layered structure leading to a reduction (increase) of the potential with respect to the perfect crystal. The difference of potentials of Fig. 11 a and Fig. 11 b is shown in Fig. 11 c representing perturbation added to the perfect crystal.

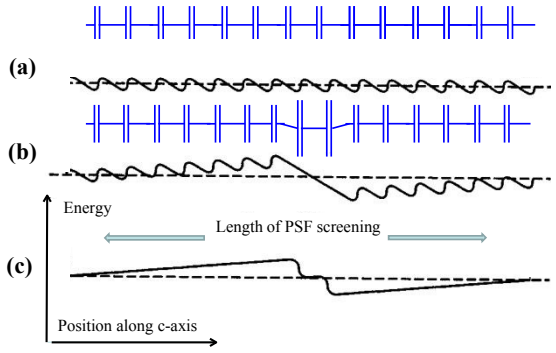

Fig. 11. Schematic presentation of potential energy in layered crystal along c-direction (a) in perfect layered structure and (b) in structure with a double PSF. The difference of potentials is shown in (c) by contribution on a length of PSF screening.

Two important consequences follow from Fig. 11. First, because of spontaneous polarization, photo-excited charges of different type can be re-sandwiched almost instantly after a short excitation pulse if the diffusion length $(D_{\perp}t)^{0.5}$ exceeds a double layers distance. By this effect the bottom of the indirect conduction band is pulling into the lower state and the top of the valence band is pushing up that provides stabilization for charge localization since four Tl-S interlayer bonds acting against two ones (see Fig. 1 right) and favors the charge separation. The process may be represented by torsional vibrations of the InS_4 tetrahedra with one of their axis in the In-S layers and fluctuations of local electric field gradient.[15] Particle segregation on the layer plane thus produces Stokes shift between the

View Article Online
DOI: 10.1039/C8CP06209A

absorbed and emitting exciton (Fig. 5). We expect that separation of charge type in neighboring layers reduces the BGN effect as well as probability of the Auger recombination. From Fig. 11 c it could be pointed out that PSF disturbs the short dipole separated moments by carrier further diffusion toward the PSF center. Thus, we felt that frequent PSF appearance destroys geminate out-of-plain exciton and provides shorter radiative lifetime.

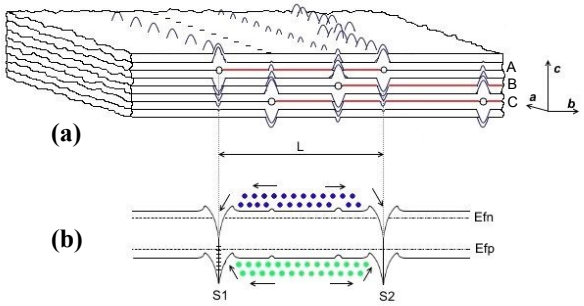

Fig. 12. (a) Schematic presentation of layered structure with an exaggerated c-axis scale. The horizontal lines represent stacked layers. The PSFs length *L* is indicated in red. Its edges (open symbols) provide stress and distortion on nearby layers. (b) The band-bending model with excess electrons (blue) and holes (green) situated in parallel layer interface. The quasi Fermi levels of carriers determine bipolar flow to the recombination sinks (S1, S2).

Fig. 12 a shows schematic fragment of layered sandwiched structure. We assume that PSFs arbitrary occur on certain depths. The average length of PSF, *L,* is indicated by solid red line. The edges of PSF behave as physically stress distortion regions which act on the neighboring layers. We assume that interfacial states at PSF edge are introduced by residual impurities, inclusions or clusters. The states depending of their donor and acceptor like character are the cause of the energy band downwards or upwards acting as strong recombination sink. If certain PSF edges overlap, a block wall is expected to occur in a real crystal. These blocks can be observed on cleaved layered crystal surfaces as fragments of platforms. The inspection by optical microscope shows that the most preferred walls directions are aligned with *a*- or *b*- crystallographic axes, as indicated in Fig. 12 a.

In Fig. 12 b we present the band diagram where excess electrons and excess holes are localized on neighboring planes with the corresponding quasi-Fermi levels E_{Fn} and E_{Fp}. The nearest PSF (marked A) makes the strongest stress perturbation on the top layer in Fig. 12 a while sufficiently smaller perturbations occur from two deeper ones marked as B and C. For the long *L*, we expect the sufficient number of weak stress distortions within length of PSF. Only two small ones are shown in Fig. 12 a for simplicity.

Furthermore, we consider the screening effects. As noted before, the easy screening of a depolarization field is performed by photo-excited carriers themselves. For a low excitation the screening effect is small and particles need to overcome temporal distortions in the layer plane until reach the recombination sink. One way to accelerate this process is a round bypasses within the same layer with higher diffusivity $D_{\|}$, and another - bypasses across the layers with sufficiently lower diffusivity $D_{\perp}$. The screening of stresses at high excitation is expected allowing maximal diffusion in the layer plane.

From the other hand, at high excitation a non-negligible internal electric field due to charge separation between planes will occur. Such Stark field is a driving force for phase reconstruction in the interlayer. We assume that field provides hybridization in Tl^+ ion arrangement similar to that occurring within I-phase with quadrupling of the lattice unit.[11] We undertake that the phase transition is reversible for medium excitation of 10-15 mJ/cm^2 due to slow charge leakage from phase transition

View Article Online
DOI: 10.1039/C8CP06209A

region (Fig. 9 a). For even higher excitation level, the electric field provides enough strain for permanent crystal phase transformation (Fig. 9 b).

By these calculations we make a deduction that the lifetime and the diffusivity at high injections are ruled by the third carrier decay component. According to our model (Fig. 12 a), this component relies on the stresses (layer corrugation) provided by often distribution of PSFs in the structure. The favorable diffusion condition occurs at very high *e-h* pair generation with a screening of the PSF subsystem. The *Erbium* in $TlInS_2$ allows perfect avoiding this component even for a medium excitation range for much rear PSF incorporation in the structure. As a consequence, the out-off-layer excitons may migrate to the layer sink and recombine by much shorter time. A bipolar relation between radiative and nonradiative lifetime of carrier plasma can become satisfied then. The impact of the *Erbium* atom on the PSF incorporation can be understood if Er atom is chemically incompatible with the host structure (no impurity substitution signs are obtained). Then the enhanced segregation of Er clusters prevents frequent PSFs during the extended cooling time of the growth crystal pull-out.[24] In Supplementary file (SI. 4) we provide calculations of the diffusion length based on measured lifetime and diffusion coefficient presented in Fig. 7. This calculation validates that diffusion length is about 0.7 μm, very similar in both type of $TlInS_2$ crystals and nearly excitation independent. Thus, only the frequency of PSFs distribution in depth can be associated to PL enhancement and variation of nonradiative lifetime.

In the recent paper [6] Seyidov et. al. provided results of investigation in the *Lanthanum* 0.3 mol % doped $TlInS_2$ in a perpendicular external electric field, *E*. They showed that dielectric polarization, *P,* is fully different from that in the undoped $TlInS_2$. They also displayed that poling in *P-E* hysteresis and saturation of polarization at high electric field in the *Lanthanum* doped $TlInS_2$ was sufficiently smaller in any phase and temperature range. This result allows making a conclusion that the *Erbium* in our case is not the exceptional impurity. Some other chemically inactive atoms, like *Lanthanium* or others,[24] inserted in small amount in the melt may decrease the frequency of PSF creation and change the crystal memory effects. In our work we definitely show that the diffusivity is related to rather rear PSF incorporation in the layers of $TlInS_2$(Er).

Finally, the driving force of *e-h* separation is caused by interlayer atoms (Tl^+ and S) reconfiguration providing shift of band gap edges in the CBM and VBM. While interlayer bonding is weak, external perturbation can cause the modification of interlayer bonding by sliding of Tl^+ away from [110] and [1,-10] directions and reinforcing Tl^+-Tl^+ interaction. This is a kind of hybridization of electron lone pairs.[8,9,11] Such excess carrier separation does not exist in isotropic semiconductor crystals. The crystal phase transition by the use of light can be simply understood as a minimization of the potential energy by a sufficiently strong separation of *e-h* pairs.

The coexisting of 2D-electron and 2D-hole gas at room temperature recently has been demonstrated in high-quality $SrTiO_3/LaAlO_3/SrTiO_3$ hetero-interfaces and it was proposed that separated excitons can produce the 2D exciton liquid at low temperatures.[53] A thin phototransistor with broad-spectral response on $TlGaSe_2$ layered structure operating at RT was demonstrated [54] while the $TlGaSe_2$ ability for radiation detectors was presented in Ref. [17].

5. Summary

To conclude, time-resolved studies have been implemented for undoped and *Erbium* doped $TlInS_2$ layered crystals in accord with investigation using steady-state measurements. The metastable/permanent phase transformation appearing at the high pulse excitation has been discovered for the first time. The measurements indicate a number of similarities in two types of investigated $TlInS_2$ crystals. These are identical Raman spectra, similar shape and spectral position of PL, linear recombination and increasing diffusivity at high excitation with suppression/absence of Auger recombination and BGN effect as well as small surface recombination due to restricted diffusion across the layers. At the same time, a few important dissimilarities have been discovered. These are a large PL efficiency difference related to radiative lifetime damping in undoped $TlInS_2$ in correlation to stretch-exponential component which produces injection dependence of carrier lifetime and diffusivity.

View Article Online
DOI: 10.1039/C8CP06209A

We have followed the progress towards understanding of layered crystals structure by introducing a general polarization layered crystal model which allows explaining the experimental features. The model invokes two main consequences. First, an ability of charge separation between neighboring layers as a result of the sawtooth potential of spontaneous polarization with a depolarization field in c-axis direction. This feature provides out-of-plane geminate exciton creation over a period of 10 ps. Second, a presence of common PSF structural defect arbitrary implemented in layers during the crystal growth. The PSF edges are acting as recombination sink for a fast linear recombination at high excitation. The PSFs edge also provides internal stresses in neighboring layers which, according to our model, is responsible for occurrence of the stretched-exponential excess carrier decay. In turn, the *Erbium* doped $TlInS_2$ layered crystals support sufficiently less frequent PSFs implementation. Numerical modeling shows that PSF average length remains almost the same in two types of investigated crystals.

A conclusive evidence of electrons and holes separation followed by free migration along the layers is a driving force for crystal phase transformation at high excitation level. The magnitude of this effect in layered crystal and any possibility to control phase transformation still remains an open question. We just note that alike effect of adaptive light collection with self-ordered polarizable particles was demonstrated in optical resonators by illumination from the side of a strong laser.[55]

Conflicts of interest

There are no conflicts to declare.

Acknowledgement

The authors gratefully acknowledge support by grant LB-17-01 “Transient optical processes in compensated silicon carbide and chalcogenide 2D semiconductors” from the Research Council of Lithuania and grant No LITG17-009 from Belarusian Republican Foundation for Fundamental Research.

View Article Online
DOI: 10.1039/C8CP06209A

References

[1] Panich AM. Electronic properties and phase transitions in low-dimensional semiconductors. J Phys Condens Matter. 2008;20:293202.
[2] Hanias MP, Anagnostopoulos AN, Kambas K, Spyridelis J. Electrical and optical properties of as-grown $TlInS_2$, $TlGaSe_2$ and $TlGaS_2$ single crystals. Mater Res Bull. 1992;27:25.
[3] Shim Y, Nishimoto Y, Okada W, Wakita K, Mamedov N. Temperature-dependent spectro-ellipsometric studies of optical transitions near absorption edge of $TlInS_2$. Phys Status Solidi C. 2008;5:1121.
[4] Gomonai OO, Rosul RR, Guranich PP, Slivka AG, Roman IYu, Rigan MYu. Growth and characterization of sulphur-rich $TlIn(S_{1-x}\text{-}Se_x)_2$ single crystals. High Press Res. 2012;32:39.
[5] Veliyev RG, Seydov MYu, Gasanov NZ, Seyidov FM. The magneto-dielectric properties of compounds and alloys in the systems of $TlInS_2$–$TlFeS_2$, $TlInS_2$–$TlFeSe_2$. J Alloys Compd. 2010;506:800.
[6] Seyidov MYu, Mikailzade FA, Suleymanov RA, Aliyeva VB, Mammadov TG, Sharifov GM. Polarization switching in undoped and La-doped $TlInS_2$ ferroelectric semiconductors. Physica B Condens Matter. 2017;526:46.
[7] Grivickas V, Gulbinas K, Gavryushin V, Bikbajevas V, Korolik OV, Mazanik AV, et al. Room-temperature photoluminescence in quasi-2D $TlGaSe_2$ and $TlInS_2$ semiconductors. Phys Status Solidi Rapid Res Lett. 2014;8:639.
[8] Yee KA, Albright ThA. Bonding and structure of $TlGaSe_2$. J Am Chem Soc. 1991;113:6474.
[9] Gulbinas K, Grivickas V, Gavryushin V. Anisotropy of band gap absorption in $TlGaSe_2$ semiconductor by ferroelectric phase transformation. Appl Phys Lett. 2014;10:5242107.
[10] Gomonnai OO, Gordan O, Guranich PP, Slivka AG, Gomonnai AV. Temperature-dependent dielectric functions and interband critical points of sulfur-rich $TlIn(S_{1-x}\text{-}Se_x)_2$ layered solid solution crystals. Appl Surf Sci. 2017;424:383.
[11] Panich AM. Nuclear exchange coupling and electronic structure of low dimensional semiconductors. Appl Magn Reson. 2004;27:29.
[12] Panich AM, Ailion DC, Kashida S, Gasanly N. Gallium and thallium NMR study of phase transitions and incommensurability in the layered semiconductor $TlGaSe_2$. Phys Rev B. 2004;69:245319.
[13] Panich AM, Mogilyansky D, Sardarly RM. Phase transitions and incommensurability in the layered semiconductor $TlInS_2$ – an NMR study. J Phys Condens Matter. 2012;24:135901.
[14] Seyidov MYu, Suleymanov RA, Acar E, Odrinsky AP, Mammadov TG, Nadjafov AI, et al. Photoelectric activity of defects in La-doped layered $TlInS_2$ crystals. J Low Temp Phys. 2014;40:830.
[15] Seyidov MYu, Suleymanov RA, Sale Y, Balaban E. Enhanced excitonic photoconductivity due to built-in internal electric field in $TlGaSe_2$ layered semiconductor. J Appl Phys. 2014;116:213702.
[16] Seyidov MYu, Suleymanov RA, Odrinsky AP, Nadjafov AI, Mammadov TG, Samadli EG. Photoinduced current transient spectroscopy of $TlInS_2$ layered crystals doped with Er, B, and Tb impurities. Jpn J Appl Phys. 2011;50:05FC08.
[17] Johnsen S, Liu Z, Peters JA, Song J-H, Peter SC, Malliakas CD, et al. Thallium chalcogenide-based wide-band-gap semiconductors: $TlGaSe_2$ for radiation detectors. Chem Mater. 2011;23:3120.
[18] Orudzhev G, Dhim Y, Wakita K, Mamedov N, Jafarova S, Hashimzade F. Linearized augmented plane wave band structure calculations and dielectric function of layered $TlGaSe_2$. Jpn J Appl Phys. 2008;47:8182.
[19] Kashida S, Yanadori Y, Otaki Y, Seki Y, Panich AM. Electronic structure of ternary thallium chalcogenide compounds. Physica Status Solidi A Appl Res. 2006;203:2666.
[20] McMorrow DF, Cowley RA, Hatton PD, Banys J. The structure of the paraelectric and incommensurate phases of $TlGaSe_2$. J. Phys.: Condens. Matter **2**, 3699 (1990).
[21] Grivickas V, Odrinski A, Bikbajevas V, Gulbinas K. Carrier trapping and recombination in $TlGaSe_2$ layered crystals. Phys Status Solidi B Basic Res. 2013;250:160.
[22] Ozdemir S, Bucurgat M. Characteristics of traps in $TlInS_2$ single crystals. Curr Appl Phys. 2013;13:19.
[23] Arai T, Aoyagi J, Maryama Y, Onari S, Allakhverdiev KR, Bairamova E. Photoluminescence of $TlInS_2$ at low temperatures. Jpn J Appl Phys. 1993;32 (Suppl 32-3):754.
[24] Korolik OV, Kaabi SA, Gulbinas K, Mazanik AV, Drozdov NA, Grivickas V. Band edge photoluminescence of undoped and doped $TlInS_2$ layered crystals. J Lumin. 2017;187:507.
[25] Gasanly NM. Band gap and refractive index tunability in thallium based layered mixed crystals. J Appl Phys. 2015;118:035118.
[26] Shim Y, Okada W, Wakita K, Mamedov N. Refractive indices of layered semiconductor ferroelectrics $TlInS_2$, $TlGaS_2$, and $TlGaSe_2$ from ellipsometric measurements limited to only layer-plane surfaces. J Appl Phys. 2007;102:083537.

View Article Online
DOI: 10.1039/C8CP06209A

[27] Gnatenko YuP, Furyer MS, Bukivskii AP, Tarakhan LM, Gamernyk RV. Photoluminescence and photoelectric properties of CdTe crystals doped with Er atoms. J Lumin. 2015;160:258.
[28] Isik M, Gasanly NM, Korkmaz F. Multiphonon absorption processes in layered structured $TlGaS_2$, $TlInS_2$ and $TlGaSe_2$ single crystals. Physica B Condens Matter. 2013;421:50.
[29] Gomonnai AV, Petryshynets I, Azhniuk YuM, Gomonnai OO, Roman IYu, Turok II, et al. Growth and characterisation of sulphur-rich $TlIn(S_{1-x}Se_x)_2$ single crystals. J Cryst Growth. 2013;367:35.
[30] Ščajev P, Kato M, Jarašiūnas K. A diffraction-based technique for determination of interband absorption coefficients in bulk 3C-, 4H- and 6H-SiC crystals. J Phys D Appl Phys. 2011;44:365402.
[31] Fowles GR. Introduction to Modern Optics. New York: Dover Publications; 1975. 336 p.
[32] Eichler HJ, Gunter P, Pohl DW. Laser-induced dynamic gratings. Springer Series in Optical Sciences. V50. Berlin: Springer-Verlag: 1986. 256 p.
[33] Hoffman CA, Jarašiūnas K, Gerritsen HJ, Nurmikko AV. Measurement of surface recombination velocity in semiconductors by diffraction from picosecond transient free-carrier gratings. Appl Phys Lett. 1978;33:536.
[34] Jarasiunas K, Aleksiejunas R, Malinauskas T, Gudelis V, Tamulevicius T, Tamulevicius S, et al. Implementation of diffractive optical element in four-wave mixing scheme for *ex situ* characterization of hydride vapor phase epitaxy-grown GaN layers. Rev Sci Instrum. 2007;78:33901.
[35] Linnros J, Grivickas V. Carrier diffusion measurements in silicon with a Fourier transient grating method. Phys Rev B Condens Matter. 1994;50:16943.
[36] Grivickas P, Grivickas V, Linnros J, Galeckas A. Fundamental band edge absorption in nominally undoped and doped 4H-SiC. J Appl Phys. 2007;101:123521.
[37] Allakhverdiev KR. Two-photon absorption in layered $TlGaSe_2$, $TlInS_2$, $TlGaS_2$ and GaSe crystals. Solid State Commun. 1999;111:253.
[38] Zhang XB, Taliercio T, Kolliakos S, Lefebvre P. Influence of electron–phonon interaction on the optical properties of III nitride semiconductors. J Phys Condens Matter. 2001;13:7053.
[39] Klein PB. Carrier lifetime measurement in $n-$ 4H-SiC epilayers. J Appl Phys. 2008;103;033702.
[40] Linnros J, Lalic N, Galeckas A, Grivickas V. Analysis of the stretched exponential photoluminescence decay from nanometer-sized silicon crystals in SiO_2. J Appl Phys. 1999;86:6128.
[41] Malinauskas T, Nargėlas S, Aleksiejūnas R, Jarašiūnas K. Heterodyne detection scheme for light-induced transient grating experiment. Opt Commun. 2008;281:6061.
[42] Shank CV, Yen R, Hirlimann C. Time-resolved reflectivity measurements of femtosecond-optical-pulse-induced phase transitions in silicon. Phys Rev Lett. 1983;50:454.
[43] Rethfeld B, Sokolowski-Tinten K, Von Der Linde D, Anisimov SI. Timescales in the response of materials to femtosecond laser excitation. Appl Phys A Mater Sci Process. 2004;79:767.
[44] Linnros J, Grivickas V. Carrier lifetime: free carrier absorption, photoconductivity and photoluminescence. In: Kaufmann EN, editor. Characterization of Materials. 2nd ed. N.Y,: John Wiley and Sons Publication; 2012. p. 427-456.
[45] Grivickas P, Grivickas V, Linnros J. Excitonic absorption above the Mott transition in Si. Phys Rev Lett. 2003;91:246401.
[46] Ščajev P, Jarašiūnas K. Temperature- and excitation-dependent carrier diffusivity and recombination rate in 4H-SiC. J Phys D Appl Phys. 2013;46:265304.
[47] Ščajev P, Malinauskas T, Lubys L, Ivakin E, Haenen M, Jarašiūnas K. Optical monitoring of nonequilibrium carrier diffusion in single crystalline CVD and HPHT diamonds under high optical excitation. Phys Status Solidi Rapid Res Lett. 2011;5:193.
[48] Persson C, Lindefelt U, Sernelius BE. Band gap narrowing in *n*-type and *p*-type 3C-, 2H-, 4H-, 6H-SiC, and Si. J Appl Phys. 1999;86:4419.
[49] Grivickas V, Thungström G, Bikbajevas V, Linnros J, Noreika D. Characterization of Si wafer bonding by injection-dependent recombination velocity. Jpn J Appl Phys. 1995;34:L806.
[50] Qasrawi AF, Gasanly NM. Investigation of carrier scattering mechanisms in $TlInS_2$ single crystals by Hall effect measurements. Cryst Res Technol. 2004;39:439.
[51] Allakhverdiev KR, Mammadov TG, Suleymanov RA, Gasanov NZ. Deformation effects in electronic spectra of the layered semiconductors $TlGaS_2$, $TlGaSe_2$ and $TlInS_2$. J Phys Condens Matter. 2003;15:1291.
[52] Iwata H, Lindefelt U, Oberg S, Briddon PR. Ab initio study of 3C inclusions and stacking fault–stacking fault interactions in 6H-SiC. J Appl Phys. 2003;93:1577.
[53] Lee H, Campbell N, Lee J, Asel TJ, Paudel TR, Zhou H, et al. Direct observation of a two-dimensional hole gas at oxide interfaces. Nature Mater. 2018;17:231.

View Article Online
DOI: 10.1039/C8CP06209A

[54] Yang S, Wu M, Wang H, Cai H, Huang L, Jiang C, et al. Ultrathin ternary semiconductor $TlGaSe_2$, phototransistors with broad-spectral response. 2D Mater. 2017;4:035021.
[55] Torggler V, Ritsch H. Adaptive multifrequency light collection by self-ordered mobile scatterers in optical resonators. Optica. 2014;1:336.

Paper

Carrier dynamics in highly-excited $TlInS_2$: Evidence of 2D electron-hole charge separation at parallel layers

Vytautas Grivickas, Patrik Ščajev, Vitalijus Bikbajevas, Olga V. Korolik and Alexander V. Mazanik

Imprinted transient grating fringes in $TlInS_2$ are attributed to new crystal phase formed by 2D electron-hole charge separation on local layers